THE JOURNAL OF PHYSICAL CHEMISTRY LETTERS
A JOURNAL OF THE AMERICAN CHEMICAL SOCIETY

pubs.acs.org/JPCL Letter

Hybrid Quantum-Classical Boson Sampling Algorithm for Molecular Vibrationally Resolved Electronic Spectroscopy with Duschinsky Rotation and Anharmonicity

Yuanheng Wang, Jiajun Ren, Weitang Li, and Zhigang Shuai*

Cite This: J. Phys. Chem. Lett. 2022, 13, 6391−6399 Read Online

ACCESS | Metrics & More | Article Recommendations | Supporting Information

ABSTRACT: Using a photonic quantum computer for boson sampling has demonstrated a tremendous advantage over classical supercomputers. It is highly desirable to develop boson sampling algorithms for realistic scientific problems. In this work, we propose a hybrid quantum-classical sampling (HQCS) algorithm to calculate the optical spectrum for complex molecules considering Duschinsky rotation effects and anharmonicity. The classical sum-over-states method for this problem has a computational complexity that exponentially increases with system size. The HQCS algorithm creates an intermediate harmonic potential energy surface (PES) to bridge the initial and final PESs. The magnitude and sign of the overlap between the initial and the intermediate state are estimated by boson sampling and classical algorithms, respectively. The overlap between the intermediate and the final state is efficiently evaluated by classical algorithms. The feasibility of HQCS is demonstrated in calculations of the emission spectrum of a Morse model as well as the pyridine molecule.

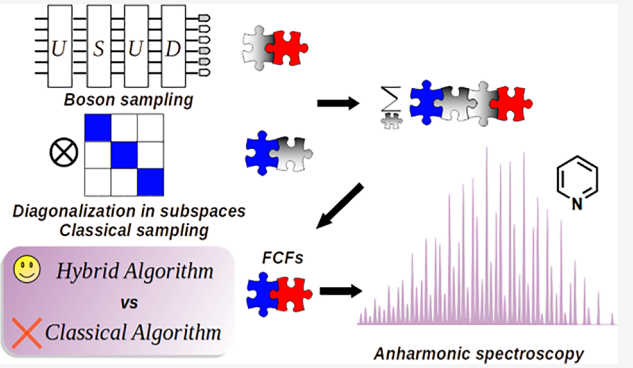

In the early 1980s, Feynman proposed quantum computation as a natural solution for many-body problems too hard for classical computers.[1] Since then, many quantum algorithms have been devised to solve classically hard problems. However, the presently known methods such as Shor's algorithm[2] for factorization and quantum phase estimation (QPE)[3] for the eigenvalue problems require an error-tolerant quantum computer, which will not be available in the near future. Variational quantum algorithms[4] hybridizing classical and quantum computation are regarded as a practical choice for quantum computation applications with the current noisy intermediate-scale quantum (NISQ) device. On the other hand, quantum computational advantage has been reported through quantum sampling algorithms such as random circuit sampling,[5] boson sampling,[6,7] and its variant, Gaussian boson sampling (GBS).[8−11] In the last year, the quantum computer "Jiu Zhang 2.0"[9,10] performed GBS on an $\sim 10^{43}$ large Hilbert space which was shown to be $\sim 10^{24}$ faster than a brute-force simulation on state-of-the-art classical computers. Recently, the boundary of quantum advantage of GBS was identified,[12] and the evidence for the hardness of GBS was provided.[13] Currently, it is valuable to develop algorithms that profit from the quantum computational advantage of the quantum sampling algorithms and devices to solve real-world problems.

Here, we focus on the computation of a molecular vibrationally resolved electronic spectrum taking both the Duschinsky rotation (DR) and anharmonicity into account. DR refers to the mode mixing between normal vibrational modes on the initial and final potential energy surface (PES) for the electron transition.[14−16] It helps to more accurately characterize the difference between the initial and final PES rather than just considering the displacement between the two equilibrium geometries along each mode. Meanwhile, it couples the vibrational modes and thus results in entangled many-body problems that need to be solved in the whole Hilbert space, which is exponentially large with the number of modes. Several experimental[17−21] and theoretical[22,23] works have focused on the simulation of the molecular spectrum with the DR effect and under harmonic approximation using the boson sampling algorithms. Those works proposed to solve this problem through the time-independent (TI) approach, which is hard for classical computers with brute force.[24,25] However, it should be noted that, through the time-dependent (TD) approach, such a problem has been solved exactly and analytically on classical computers by Peng et al. back in 2007,

Received: May 16, 2022
Accepted: July 7, 2022

https://doi.org/10.1021/acs.jpclett.2c01475
J. Phys. Chem. Lett. 2022, 13, 6391−6399

and this approach was named the thermal vibration correlation function (TVCF) method.[15,26] Over the years, TVCF has been successfully used to simulate vibrationally resolved electronic spectra of complex real-world molecules.[27−29] Hence, we believe quantum computation could hardly outperform classical computation in a problem already classically efficient. Besides the DR effect, the anharmonic effect on the molecular spectrum has also been found to be very important in general for complex molecules, especially for flexible molecules.[30−32] To calculate the spectrum with both anharmonicity and DR is indeed a hard problem for classical algorithms because generally there is no analytical solution and the brute-force numerical approach has an exponential scaling with the number of modes. Therefore, it is necessary to develop quantum algorithms for such a problem, while no near-term solution has been proposed yet. The previously suggested boson sampling algorithms can only simulate Franck−Condon factors (FCFs) between harmonic states, so they are not suitable for the anharmonic spectrum. QPE based solutions have been reported to calculate the anharmonic spectrum[33] but are unable to realize with the NISQ device. The quantum simulation of quantum dynamics could be another approach toward the spectrum. Recently, a workflow was proposed to solve the condensed-phase spectrum through this approach.[34] Meanwhile, the vibrations are considered from the nuclear motion in classical molecular dynamics. Vibrational relaxation of the anharmonic Hamiltonian using vibrational perturbation theory to consider influence from all third derivatives and the semidiagonal quartic derivatives had been simulated using nonlinear optics in analogue quantum simulation,[35] but this method cannot deal with more general anharmonic PES. Generally, we should perform a quantum simulation with enough time for a converged spectrum. The accumulation of the error as the simulation time becomes longer could be a potential problem for long-time quantum simulations without error correction schemes.[36,37]

In this work, we propose a hybrid quantum-classical sampling (HQCS) algorithm to calculate the molecular vibrationally resolved electronic spectrum, including both the anharmonic effect and the DR effect. We first present an analysis of the computational complexity for this classically hard problem. Second, we will describe the HQCS algorithm in detail, which includes three subcomponents. The effectiveness of this HQCS algorithm is then demonstrated by calculating the emission spectrum of a 2-mode model as well as a pyridine molecule using a simulator for a photonic quantum computer. We believe that the real quantum device can accelerate the calculations in the near term.

The molecular vibrationally resolved electronic spectrum is commonly calculated under the Born−Oppenheimer approximation,[38] in which two adiabatic electronic states are considered, denoted with subscript "i/f" for the initial/final electronic state (symbols without a subscript refer to a general state). With mass-weighted rectilinear coordinates, the Hamiltonian can be expressed as

$$\hat{H}_0 = \sum_{n=1}^{N} -\frac{1}{2}\frac{\partial^2}{\partial q_n^2} + \begin{bmatrix} V_f(\mathbf{q}) & 0 \\ 0 & V_i(\mathbf{q}) \end{bmatrix} \tag{1}$$

where N is the total number of modes. $\mathbf{q} \equiv \{q_1, q_2, ..., q_N\}$ indicates that the PES V is a multidimensional function. For semi-rigid molecules, it is preferred to express PES in the normal coordinates, because the mode coupling in this coordinate system is minimized. The two sets of normal coordinates of the initial and final PESs are related by the DR matrix $\mathbf{S}$ and the normal-mode-projected displacement $\Delta\mathbf{q}$.

$$\mathbf{q}_f = \mathbf{S}\mathbf{q}_i + \Delta\mathbf{q}_f \tag{2}$$

The lowest order approximation to PES is the harmonic approximation,

$$V = \sum_n \frac{1}{2}\omega_n^2 q_n^2 + V_{eq} \tag{3}$$

Beyond that, the PES can be hierarchically expanded as 1-mode terms, 2-mode terms, 3-mode terms, *etc.*, which is known as the n-mode representation (n-MR).[39,40] In this work, we only consider 1-MR PES, in which the intramode anharmonicity is included and the modes are still independent of one another.

$$V = \sum_n V_n(q_n) + V_{eq} \tag{4}$$

With Fermi's golden rule and Condon's approximation, the optical transition rate at zero temperature is

$$\sigma_{abs/emi}(E) = |\mu_{if}|^2 \sum_{\mathbf{v}_f} |\langle \phi_i^{\mathbf{0}}(\mathbf{q}_i)|\phi_f^{\mathbf{v}_f}(\mathbf{q}_f)\rangle|^2 \delta(E_{f,\mathbf{v}_f} + E - E_{i,\mathbf{0}}) \tag{5}$$

$|\phi_{i/f}^{\mathbf{v}_{i/f}}\rangle$ is the initial/final vibrational state with configuration $\mathbf{v}_{i/f}$. μ_{if} is the transition dipole moment. At zero temperature, the harmonic approximation is reasonable for V_i but is inappropriate for V_f, because the optical transition starts from the equilibrium geometry of the initial state, which, however, could be far from the equilibrium geometry of the final state if the electron-vibration coupling is large. Therefore, in this work, V_i is described by a harmonic PES (eq 3) and V_f is described by a 1-MR PES (eq 4).

Unlike the harmonic spectrum with an analytical solution, no accurate and efficient classical algorithm for the anharmonic spectrum has been proposed yet to calculate eq 5. The computational cost of the sum-over-states algorithm will exponentially increase with the system size for the following two reasons. First, the numerical multidimensional integration of each FCF $|\langle \phi_i(\mathbf{q}_i)|\phi_f(\mathbf{q}_f)\rangle|^2$ generally has a computational cost exponential with the number of entangled modes on the classical computer. Second, the summation over $\mathbf{v}_f$ is also an exponentially hard problem for classical computers, because the Hilbert space increases exponentially with the system size (if d vibrational states are considered in each of the N modes, the number of $\mathbf{v}_f$ is d^N). Here, we propose a hybrid quantum-classical sampling (HQCS) algorithm to speed up these two exponentially hard problems.

The key to the HQCS algorithm is to build an intermediate harmonic PES, $V_m = \sum_n \frac{1}{2}\omega_{m,n}{}^2 q_{m,n}{}^2$, and insert its complete eigenbasis set into eq 5. $|\phi_i^{\mathbf{0}}(\mathbf{q}_i)\rangle$ and $|\phi_m^{\mathbf{v}_m}(\mathbf{q}_m)\rangle$ are harmonic wave functions, and $|\phi_f^{\mathbf{v}_f}(\mathbf{q}_f)\rangle$ is the anharmonic wave function. We call $\langle \phi_i^{\mathbf{0}}(\mathbf{q}_i)|\phi_m^{\mathbf{v}_m}(\mathbf{q}_m)\rangle$ the harmonic overlap and $\langle \phi_m^{\mathbf{v}_m}(\mathbf{q}_m)|\phi_f^{\mathbf{v}_f}(\mathbf{q}_f)\rangle$ the anharmonic overlap.

$$\sigma_{abs/emi}(E) = |\mu_{if}|^2 \sum_{\mathbf{v}_f} |\sum_{\mathbf{v}_m} \langle \phi_i^{\mathbf{0}}(\mathbf{q}_i)|\phi_m^{\mathbf{v}_m}(\mathbf{q}_m)\rangle\langle \phi_m^{\mathbf{v}_m}(\mathbf{q}_m)|\phi_f^{\mathbf{v}_f}(\mathbf{q}_f)\rangle|^2 \delta(E_{f,\mathbf{v}_f} + E - E_{i,\mathbf{0}}) \tag{6}$$

https://doi.org/10.1021/acs.jpclett.2c01475
J. Phys. Chem. Lett. 2022, 13, 6391−6399

It seems that the evaluation of eq 6 is even more complicated compared to eq 5. But, with a smart choice of the parameters of the intermediate PES and taking advantage of both quantum and classical sampling algorithms, eq 6 can be efficiently calculated. The two requirements of V_m are

(i) $\omega_{m,n} = \max(\omega_{f,n}, \omega_{i,n})$;
(ii) $\mathbf{q}_m = \mathbf{q}_f$.

With this intermediate PES, there are three steps to evaluate eq 6, which are

1. estimation of $\langle\phi_i^{\mathbf{0}}(\mathbf{q}_i)|\phi_m^{\mathbf{v}_m}(\mathbf{q}_m)\rangle$;
2. estimation of $\langle\phi_m^{\mathbf{v}_m}(\mathbf{q}_m)|\phi_f^{\mathbf{v}_f}(\mathbf{q}_f)\rangle$;
3. summation over $\mathbf{v}_m$ and $\mathbf{v}_f$.

Figure 1 shows a schematic flowchart of HQCS. The first requirement is the key to approximating the sign of

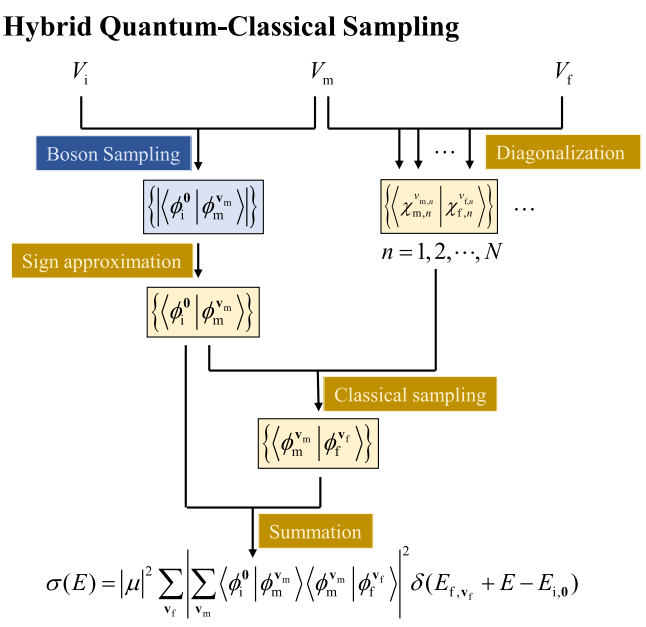

Figure 1. Schematic flowchart of the Hybrid Quantum-Classical Sampling algorithm calculating the optical spectroscopy for the transition from harmonic PES V_i to anharmonic and Duschinsky-rotated PES V_f by introducing a harmonic and Duschinsky-rotated PES V_m. Blue steps are performed on the quantum device, while yellow steps are performed on the classical computer.

$\langle\phi_i^{\mathbf{0}}(\mathbf{q}_i)|\phi_m^{\mathbf{v}_m}(\mathbf{q}_m)\rangle$. The second requirement is to make the estimation of $\langle\phi_m^{\mathbf{v}_m}(\mathbf{q}_m)|\phi_f^{\mathbf{v}_f}(\mathbf{q}_f)\rangle$ much more efficient. In the following, we replace $\mathbf{q}_m$ with $\mathbf{q}_f$ for simplicity. The Dirac delta function in eq 6 is broadened with the Gaussian function $\delta(E_{f,\mathbf{v}_f} + E - E_{i,\mathbf{0}}) \to e^{-\frac{(E-E_{i,\mathbf{0}}+E_{f,\mathbf{v}_f})^2}{2\sigma^2}}$.

The first step is the estimation of harmonic overlap $\langle\phi_i^{\mathbf{0}}(\mathbf{q}_i)|\phi_m^{\mathbf{v}_m}(\mathbf{q}_f)\rangle$. Here we calculate the magnitude using boson sampling on a quantum device, and we calculate the sign $(-1 \text{ or } +1)$ using a classical algorithm. The Doktorov unitary operator $\hat{\mathbf{U}}_{Dok}$ describes the transformation from a harmonic state expressed on its normal coordinates to the same state expressed on another set of normal coordinates.[41,42] The expression of $\hat{\mathbf{U}}_{Dok}$ can be found in the literature[43,44] (see the Supporting Information for more details). Hence, the FCFs can be expressed as

$$|\langle\phi_i^{\mathbf{0}}(\mathbf{q}_i)|\phi_m^{\mathbf{v}_m}(\mathbf{q}_f)\rangle|^2 = |\langle\varphi_i^{\mathbf{0}}(\mathbf{R}_i)|\varphi_m^{\mathbf{v}_m}(\mathbf{R}_f)\rangle|^2 = |\langle\varphi_i^{\mathbf{0}}(\mathbf{R}_f)|\hat{\mathbf{U}}_{Dok}|\varphi_m^{\mathbf{v}_m}(\mathbf{R}_f)\rangle|^2 \quad (7)$$

where $\mathbf{R}$ is the dimensionless normal coordinates. ($\mathbf{R} = \omega^{1/2}\mathbf{q}$ and $\phi(\mathbf{q}) = \varphi(\mathbf{R})$.) The right-hand side of eq 7 can be interpreted as the sampling probability P of one specific output harmonic state $|\phi_m^{\mathbf{v}_m}\rangle$ for an input harmonic state $|\phi_i^{\mathbf{0}}\rangle$ passing through an interferometer accounted by unitary transformation $\hat{\mathbf{U}}_{Dok}$ during the boson sampling process. So, the boson sampling[22,23] can be used here. The sampling probabilities $P_{\mathbf{v}_i \to \mathbf{v}_m}$ correspond to the magnitude of FCFs as

$$|\langle\phi_i^{\mathbf{0}}(\mathbf{q}_i)|\phi_m^{\mathbf{v}_m}(\mathbf{q}_f)\rangle| = \sqrt{P_{\vec{\mathbf{0}} \to \mathbf{v}_m}} \quad (8)$$

The next part is to approximate the sign. Previous works[45,46] have derived an analytic expression of the overlap between two one-mode harmonic wave functions $|\chi(q)\rangle$.The detailed analytic expression at zero temperature is given in Appendix A. From this expression and as $\omega_{m,n} = \max(\omega_{f,n}, \omega_{i,n}) \geq \omega_{i,n}$, the sign of the overlap can be calculated as eq 9.

$$\mathrm{sgn}(\langle\chi_{i,n}^{0}(q_{f,n})|\chi_{m,n}^{\nu_{m,n}}(q_{i,n})\rangle) = (\mathrm{sgn}(\Delta q_{f,n}))^{\nu_{m,n}} \quad (9)$$

Thus, for N-mode problems without DR,

$$\mathrm{sgn}(\langle\phi_i^{\mathbf{0}}(\mathbf{q}_i)|\phi_m^{\mathbf{v}_m}(\mathbf{q}_f)\rangle) = \prod_n^N (\mathrm{sgn}(\Delta q_{f,n}))^{\nu_{m,n}} \quad (10)$$

With DR, the factorized formula above is not exact anymore. However, if DR only occurs between modes with the same frequency, it will not change the sign of the overlap because the amplitude of the nodeless initial ground vibrational state is always positive. Fortunately, in molecular systems, DR commonly occurs within groups of modes having close frequencies.[47] Therefore, it can be speculated that DR could hardly flip the sign of the overlap, and thus eq 10 is still a good approximation. To verify the assumption, we calculate the sign of a two-mode and a four-mode model numerically in the Supporting Information and quantify the error of this step in each model used in this work. The results show that the assumption is quite reliable. However, it should be noted that this approximation to the sign of the overlap is only reliable for the ground vibrational state as the initial state, which limits our algorithm to the zero temperature case currently.

The second step is the estimation of anharmonic overlap $\langle\phi_m^{\mathbf{v}_m}(\mathbf{q}_f)|\phi_f^{\mathbf{v}_f}(\mathbf{q}_f)\rangle$. As the coordinates of $\phi_m^{\mathbf{v}_m}$ and $\phi_f^{\mathbf{v}_f}$ are the same and the modes are assumed to be independent, we have

$$\langle\phi_m^{\mathbf{v}_m}(\mathbf{q}_f)|\phi_f^{\mathbf{v}_f}(\mathbf{q}_f)\rangle = \prod_n \langle\chi_m^{\nu_{m,n}}(q_{f,n})|\chi_f^{\nu_{f,n}}(q_{f,n})\rangle \quad (11)$$

where $\langle\chi_m^{\nu_{m,n}}(q_{f,n})|\chi_f^{\nu_{f,n}}(q_{f,n})\rangle$ is a one-dimensional problem and thus is quite easy to calculate on classical computers. $|\chi_m^{\nu_{m,n}}(q_{m,n})\rangle$ is a one-mode harmonic wave function with analytical expression and $|\chi_f^{\nu_{f,n}}(q_{f,n})\rangle$ is a one-mode anharmonic wave function, which can be efficiently solved numerically. Practically, we use the harmonic states $\{|\chi_m^{\nu_{m,n}}\rangle\}$ with a cutoff on $v_{m,n}$ as the primitive basis set. Then we can obtain the corresponding discrete variable representation (DVR) basis set[48] and the transformation matrix between the primitive harmonic basis and the DVR basis. The matrix

https://doi.org/10.1021/acs.jpclett.2c01475
J. Phys. Chem. Lett. 2022, 13, 6391−6399

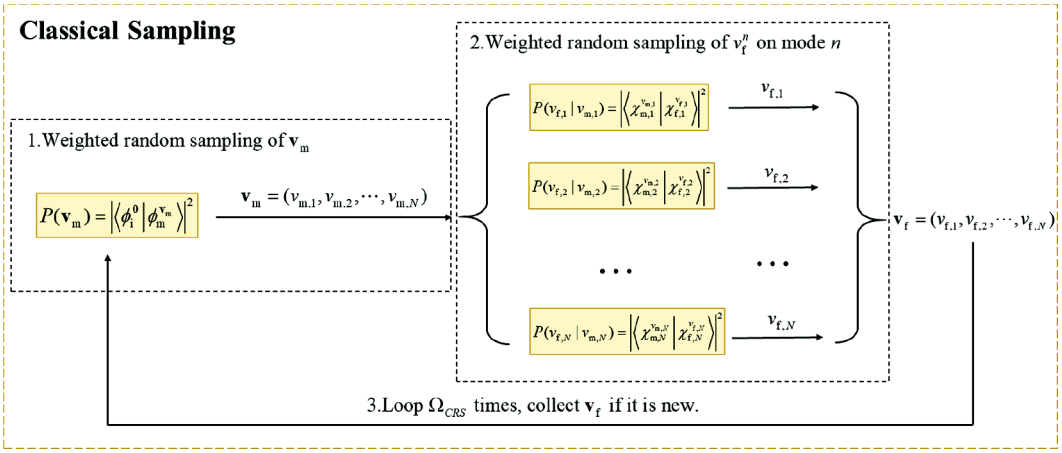

Figure 2. Schematic flowchart of the classical sampling step used in HQCS.

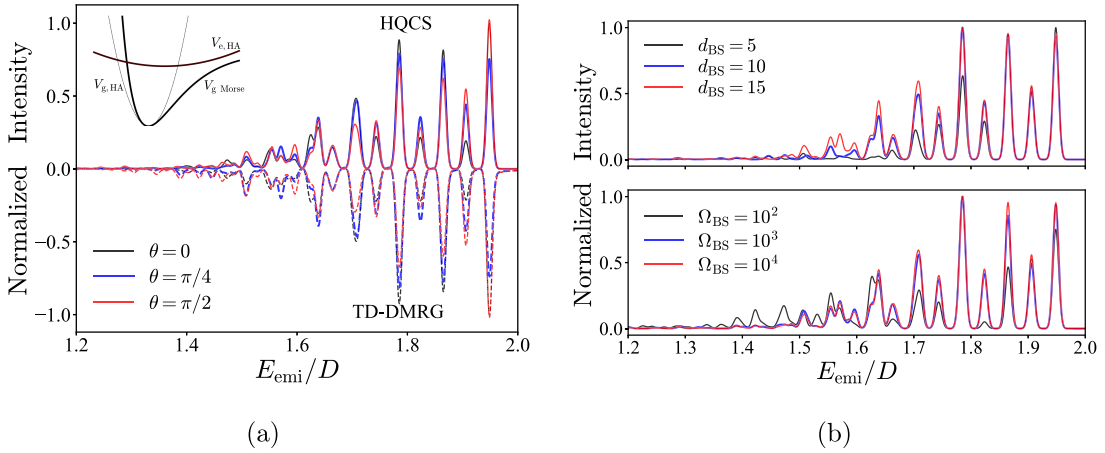

Figure 3. (a) Emission spectrum of the two-mode Morse model. The reference spectrum produced by TD-DMRG is shown on the bottom panel (dashed lines). On the top (solid lines) are results produced by HQCS. Different θ values are used to characterize the Duschinsky rotation effects. The intensity is normalized by the highest peak in the $\theta = 0$ spectrum. Inset is the schematic PES along one mode of the two-mode Morse model. The initial excited state PES $V_{e,HA}$ is harmonic (top thick line), and the final ground state PES $V_{g,Morse}$ is Morse (bottom thick line). Performing harmonic approximation on $V_{g,Morse}$ at the equilibrium point, we obtain $V_{g,HA}$ (bottom thin line), which is used as the intermediate PES. (b) Benchmark for the convergence of basis size d_{BS} of each mode (upper panel, $\Omega_{BS} = 10^4$ for all cases) and the boson sampling times Ω_{BS} (bottom panel, $d_{BS} = 5$ for all cases) in the boson sampling process.

elements of $\hat{H}_{f,n}=-\frac{1}{2}\frac{\partial^2}{\partial q_{f,n}^2}+V_{f,n}(q_{f,n})$ can be first expanded in DVR basis and then transformed to the primitive harmonic basis. Through exact diagonalizaiton of this Hamiltonian, the eigenstates $\{|\chi_f^{v_{f,n}}\rangle\}$ are obtained, and their overlaps with the primitive basis are also obtained. For an N-mode system with d basis functions for each mode, the cost of the current substep has a linear scaling with the system size, i.e., $O(Nd^3)$. It should be noted that although the total number of the anharmonic overlap $\langle\phi_m^{\mathbf{v}_m}(\mathbf{q}_f)|\phi_f^{\mathbf{v}_f}(\mathbf{q}_f)\rangle$ grows exponentially with the number of modes, only the dominant elements sampled out in the last step actually need to be calculated.

The last step is the summation over $\mathbf{v}_m$ and $\mathbf{v}_f$ in eq 6. Although the total numbers of $\mathbf{v}_m$ and $\mathbf{v}_f$ both grow exponentially with the system size, in realistic systems only a small portion of the vibrational states with large FCFs determine the vibrational structure in the electronic spectrum.[24,25] Because the boson sampling will naturally screen out $\mathbf{v}_m$ with dominant $|\langle\phi_i^0|\phi_m^{\mathbf{v}_m}\rangle|^2$, the summation over $\mathbf{v}_m$ in eq 6 will be classically efficient. Given a specific $\mathbf{v}_m$, the dominant $\mathbf{v}_f$ can also be obtained according to the weight $|\langle\chi_{m,n}^{v_{m,n}}|\chi_{f,n}^{v_{f,n}}\rangle|^2$ by a classical sampling (CS) algorithm. A schematic flowchart of CS is shown in Figure 2. It consists of Ω_{CS} sampling times. Among each time, a weighted random sampling is first performed for the intermediate vibrational state configuration $\mathbf{v}_m$ = (..., $v_{m,n}$, ...) with the weight $|\langle\phi_i^0|\phi_m^{\mathbf{v}_m}\rangle|^2$ from the boson sampling result. Then, given one $\mathbf{v}_m$, another group of weighted random samplings are carried out for all $v_{f,n}$ with the weight $|\langle\chi_{m,n}^{v_{m,n}}|\chi_{f,n}^{v_{f,n}}\rangle|^2$ calculated in the second step. After each loop, the newly appeared $\mathbf{v}_f$ = (..., $v_{f,n}$, ...) will be collected. The eventual summations over $\mathbf{v}_f$ are done only for those sampled out. The upper bound of the number of summations is $O(M_mM_f)$, where $M_{m/f}$ are the number of intermediate/final state configurations sampled by boson sampling/CS.

For some complex molecules, we may need to sample some small probability events to achieve high resolution on the spectrum. In those cases, a tunable bias $k \geq 1$ can be added to the weight for CS such that $P(v_{f,n}|v_{m,n})=\frac{|\langle\chi_{m,n}^{v_{m,n}}|\chi_{f,n}^{v_{f,n}}\rangle|^{2/k}}{\sum_{v_{f,n}}|\langle\chi_{m,n}^{v_{m,n}}|\chi_{f,n}^{v_{f,n}}\rangle|^{2/k}}$ and

https://doi.org/10.1021/acs.jpclett.2c01475
J. Phys. Chem. Lett. 2022, 13, 6391−6399

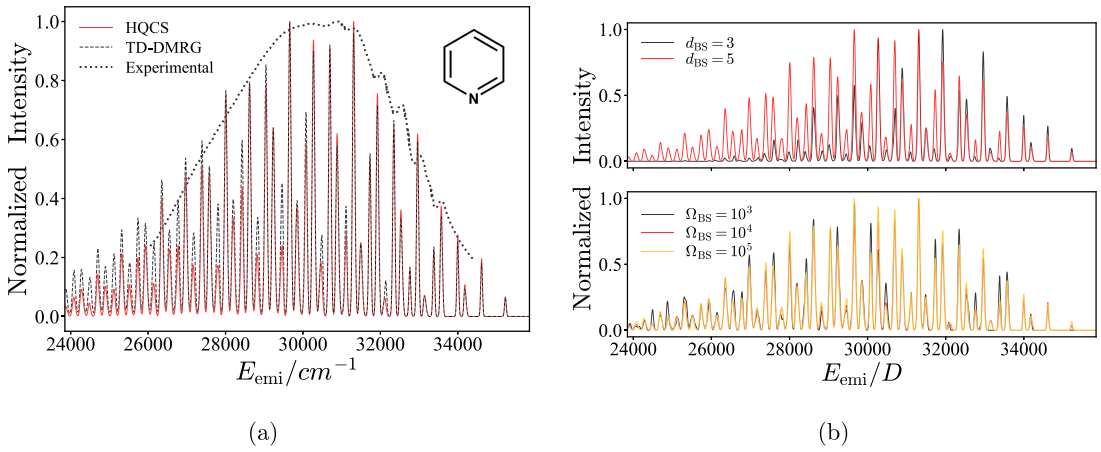

Figure 4. (a) S_1 to S_0 emission spectrum of pyridine calculated with HQCS (red solid line) and the reference result obtained by TD-DMRG (black dashed line). The anharmonic S_0 is approximated using 1-MR PES. The final state configurations $\mathbf{v}_f$ are sampled by CS with 10^4 loop times; altogether M_f = 936 different configurations of $\mathbf{v}_f$ are sampled out based on M_m = 1806 configurations of $\mathbf{v}_m$ sampled by boson sampling. The experimental result ("Experimental", black dotted curves) is also shown. The spectrum is normalized with their highest peak. The theoretical (HQCS and TD-DMRG) results have been blue-shifted by 1350 cm^{-1} for better correspondence. (b) Benchmark for the convergence of basis size d_{BS} on each mode (upper panel, $\Omega_{BS} = 10^4$ for all) and the boson sampling times Ω_{BS} (bottom panel, d_{BS} = 5 for all) in the boson sampling process.

$P(\mathbf{v}_m) = \frac{|\langle\phi_m^{\mathbf{v}_m}|\phi_f^{\mathbf{v}_f}\rangle|^{2/k}}{\sum_{\mathbf{v}_m}|\langle\phi_m^{\mathbf{v}_m}|\phi_f^{\mathbf{v}_f}\rangle|^{2/k}}$. We call it enhanced classical sampling (ECS) because it enhances the probability of sampling small probability events.

To validate the HQCS algorithm, we use the python packages "strawberry fields"[49] and "Walrus"[50] to simulate the quantum boson sampling on classical computers. The results are compared with the reference spectrum calculated by the nearly exact time-dependent density matrix renormalization group (TD-DMRG) method with the package Renormalizer[51] developed by our group; a brief introduction is in Appendix B. We calculate the emission spectrum of a two-mode model with initial excited state PES V_i as the harmonic potential and the final ground state PES V_f as the Morse potential. The intermediate PES V_m is obtained by performing the harmonic expansion at the equilibrium point on the Morse potential V_f. This model has been previously used to investigate the anharmonic effect on the internal conversion process.[52,53] The DR matrix $\mathbf{S}$ between the PESs parametrized by an angle θ is used to characterize the rotation between normal modes. More detailed parameters to construct the model, perform the HQCS calculation, and obtain the TD-DMRG reference in these two-mode models can be seen in the Supporting Information.

$$\mathbf{S} = \begin{bmatrix} \cos\theta & -\sin\theta \\ \sin\theta & \cos\theta \end{bmatrix} \tag{12}$$

In Figure 3a, the spectra from HQCS with different θ values are shown and compared with those of the TD-DMRG reference. Whether θ is 0, $\pi/4$, or $\pi/2$, the HQCS algorithm reproduces the results of TD-DMRG quite well. In Figure 3b, we explore the convergence of the basis size d_{BS} (cutoff of quanta on each mode) and sampling times Ω_{BS} for boson sampling in HQCS. We find $\Omega_{BS} = 10^4$ used here is enough while d_{BS} = 15 used here is slightly insufficient in the low energy regime. This explains the tiny deviation between HQCS and TD-DMRG in the low energy regime in Figure 3a. Moreover, we compare the sign approximated with the exact sign of the harmonic overlap from the exact diagonalization. We find the sign approximation method gives the correct sign of all involved harmonic overlaps within the basis size here. The number of signs to be compared is too high, and we have not listed them here. Similar comparisons with every exact overlap detail shown can be seen in the Supporting Information.

Furthermore, we move to the real molecular system: the S_1 to S_0 emission spectrum of pyridine. Previous studies used the perturbation method[54] to investigate the anharmonic effect of PES on the emission spectrum in this system. In our calculations, the electronic structure of pyridine and normal-mode analysis are calculated at the B3LYP/6-31g(d) level with Gaussian 16 package.[55] Following that, the DR matrix $\mathbf{S}$ and the displacement $\Delta\mathbf{q}$ are calculated by the program MOMAP[29] developed by our group. For the anharmonicity, 1-MR S_0 PES fitted with polynomial functions up to 12th order is constructed by the adaptive density-guided approach implemented in MidasCpp developed by Christiansen et al.[56] From a total of 27 normal modes, we select 7 important modes involving large displacements or the DR effect for the HQCS simulation. For the rest of the 20 modes, we only consider the difference in their zero-point energies of S_0 and S_1 PESs that shift the spectrum. Detailed information on electronic structure calculation of pyridine and the selection of important modes is given in the Supporting Information. There, the reduced 7-mode model is demonstrated to be sufficient for the emission spectrum of pyridine.

Limited by the capability of the classical simulator for boson sampling, we set d_{BS} = 5 for each mode and sampling times Ω_{BS} = 10^5 for boson sampling in HQCS here. The simulated emission spectrum from HQCS is shown in Figure 4a and compared with the TD-DMRG result (the experimental fluorescence spectrum[57] is also shown). It shows that HQCS can well reproduce the features in the spectrum while small deviations can be found in the low energy area. In Figure 4b, we find both the largest d_{BS} = 5 and the largest Ω_{BS} = 10^5 we can afford currently for classical simulation of boson sampling with no convergence. This may explain the deviations in the low energy area, similar to the case of the Morse model above.

Other potential error sources are sign approximation and classical sampling. First, we compare the approximated sign

https://doi.org/10.1021/acs.jpclett.2c01475
J. Phys. Chem. Lett. 2022, 13, 6391−6399

with the sign of the exact harmonic overlap produced by the ground state DMRG calculation. (We optimize the lowest vibrational state on the electronic excited state using the harmonic vibrational states at the electronic ground state as the basis. Then the coefficient optimized for each basis function corresponds to the overlap.) With the error defined in eq 13, we calculate the summation of FCFs whose sign is incorrectly approximated. The maximum error should be one and the minimum error should be zero.The calculated error in pyridine is only around 10^{-5}.

$$\text{Error} = \sum_{\mathbf{v}_m} \left| \frac{\prod_n^N (\text{sgn}(\Delta q_{f,n}))^{v_{m,n}} - \text{sgn}(\langle \phi_i^{\mathbf{0}}(\mathbf{q}_i) | \phi_m^{\mathbf{v}_m}(\mathbf{q}_f)\rangle)}{2} \right| \times |\langle \phi_i^{\mathbf{0}}(\mathbf{q}_i) | \phi_m^{\mathbf{v}_m}(\mathbf{q}_f)\rangle|^2 \quad (13)$$

Then we use the deviation $\eta = 1 - \sum_{\mathbf{v}_f} \sum_{\mathbf{v}_m} |\langle \phi_i^{\mathbf{0}} | \phi_m^{\mathbf{v}_m}\rangle \langle \phi_m^{\mathbf{v}_m} | \phi_f^{\mathbf{v}_f}\rangle|^2$ to measure whether the classical sampling process is converged. Table 1 shows

Table 1. Comparison between the Results from Different Sampling Times Ω_{CS} of Classical Sampling

Ω_{CS}	M_f	η
10^1	10	0.97
10^2	78	0.64
10^3	359	0.18
10^4	936	0.031
10^5	1797	0.004

the results with different Ω_{CS} values. The results indicate that the summation over 936 final configurations $\mathbf{v}_f$ from CS after 10^4 sampling times and with 1806 intermediate configurations $\mathbf{v}_m$ from the boson sampling can already give a quantitatively correct spectrum (the deviation is less than 5%). It should be noted that the size of the final configuration space for sampling is 10^7 (10 quanta for each of the 7 modes). Namely, the HQCS algorithm can vastly reduce the computational cost for the summation.

Now, we are confident that the error from both sign approximation and classical sampling are negligible in this pyridine case. As the insufficient quanta and limited sampling times of boson sampling are confirmed as the dominant error source, the errors are expected to reduce with a real boson sampling device, which can efficiency simulate enough quanta on each mode and sampling times. Nowadays, the real quantum sampling device can simulate systems with even more modes. So in Appendix C, we also give a short discussion on the scalability of sampling algorithms used.

To perform the HQCS algorithm on an actual photonic quantum device, more error sources including photon loss, noise, and distinguishability[18] should be considered. In this work, we focus on the 1-MR potential expressed on the normal mode coordinates. In real molecules, there may exist more complex situations where the anharmonic crossing terms between the normal modes are hard to ignore. We consider that a direct but less efficient treatment is to diagonalize those modes as a whole. Another system specific treatment is finding another coordinate system where the anharmonic crossing terms are small like what has been done by former studies to handle the rotation potential.[32,58] It will have many crossing terms if it is expressed with normal mode coordinates

In conclusion, we have proposed a hybrid quantum-classical sampling algorithm, combining the boson sampling on quantum devices and the classical sampling on classical computers, for simulating molecular vibrationally resolved electronic spectroscopy including both the Duschinsky rotation effect and the anharmonicity. Although the current algorithm is only for the zero temperature case and independent modes, the simplified problem is still classically hard. The effectiveness of the HQCS algorithm is demonstrated in a two-mode Morse potential model and pyridine molecule by comparing with the nearly exact TD-DMRG method. Moreover, as we have intentionally designed the HQCS algorithm to contain only one step of boson sampling that is already realized in many platforms[17−20] and three other steps on robust classical computers, we suggest HQCS is a practical near-term quantum simulation scheme to achieve quantum computational advantage for molecular spectroscopy and boost related photophysical and photochemical research.

APPENDIX A: ANALYTICAL EXPRESSION OF THE OVERLAP BETWEEN ONE-DIMENSIONAL HARMONIC STATES

$$\langle \chi_i^0 | \chi_m^{v_m} \rangle = \Gamma (\Delta q_f)^{v_m} \times \left(\sum_l C_l \right) \quad (14)$$

$$C_l = \frac{(-1)^{v_m - l} + 1}{2} (\Delta q_f)^{-(v_m - l)} \beta_m^{l/2} \frac{2^l}{l!} \left(\frac{\beta_i}{\beta_i + \beta_m} \right)^l \left(\frac{\beta_m - \beta_i}{\beta_i + \beta_m} \right)^{(v_m - l)/2} \frac{1}{\left(\frac{v_m - l}{2} \right)!}$$

$$\Gamma = \left(\frac{v_m!}{2^{v_m}} \times \frac{2\sqrt{\beta_i \beta_m}}{\beta_i + \beta_m} \right)^{1/2} \exp\left(-\frac{\beta_i \beta_m (\Delta q_f)^2}{2(\beta_i + \beta_m)} \right) \quad (15)$$

where $\beta_i = \omega_i/\hbar$ and l are non-negative integers meeting the condition $l \le v_m$. As the Γ-function is always non-negative and C_l is non-negative when $\omega_{m,n} \ge \omega_{i,n}$, the sign of the overlap only depends on the sign of the displacement Δq_f and the quanta v_m of the intermediate state.

APPENDIX B: TIME CORRELATION FUNCTION FORMALISM OF THE SPECTRUM

The spectra from TD-DMRG for the benchmark are obtained from the time correlation function (TCF) formalism. Here we will give a brief introduction. Detailed derivations can be seen from our former works.[59,60] Performing a Fourier transform of the delta function in eq 5 and then removing the completeness relation $\mathbf{I} = \sum_{\mathbf{v}_f} |\phi_f^{\mathbf{v}_f}(\mathbf{q}_f)\rangle\langle\phi_f^{\mathbf{v}_f}(\mathbf{q}_f)|$, we can obtain the TCF formalism as eq 16. By TD-DMRG, the TCF $C(t)$ is first calculated within a finite time period and then is Fourier transformed to obtain the spectrum.

$$\sigma_{\text{abs/emi}}(E) = |\mu_{if}|^2 \int_{-\infty}^{\infty} dt\ e^{-iEt} C(t)$$

$$C(t) = e^{iE_{i,0}t} \langle \phi_i^{\mathbf{0}}(\mathbf{q}_i) | e^{-i\hat{H}_f t} | \phi_i^{\mathbf{0}}(\mathbf{q}_i)\rangle \quad (16)$$

https://doi.org/10.1021/acs.jpclett.2c01475
J. Phys. Chem. Lett. 2022, 13, 6391−6399

APPENDIX C: SCALABILITY OF THE SAMPLING ALGORITHM

Though the HQCS algorithm is universal, its efficiency depends on the system. The scalability of quantum boson sampling and classical sampling in our HQCS algorithm is discussed. Inspired by the central limit theorem used by former works,[22] we assume the spectrum is in the normal distribution characterized by a mean energy E_μ indicating the center of the spectrum and a deviation variance σ proportional to the full width at half-maximum (FWHM) of the whole spectrum (for a normal distribution, FWHM $= 2\sqrt{2\ln 2}\sigma$). Here, the standard error of the mean (center of the spectrum) sampled is related to the sampling times Ω by $\epsilon_{SE} = \sigma/\sqrt{\Omega}$. To keep ϵ_{SE} a small constant, Ω should be proportional to σ^2. This indicates that as long as the width of the spectrum remains the same, the sampling times required to keep a given ϵ_{SE} will not increase even when the system size N grows. A practical case requiring larger sampling times is the spectrum for the low-frequency mode with a very large Huang−Rhy factor. The FWHM of the spectrum could be similar to the high-frequency mode with a smaller Huang−Rhy factor. Meanwhile, the ϵ_{SE} should be smaller to distinguish between the vibrational structures on the spectrum. Thus, more sampling times are required. We consider this result to be consistent with experience. For the low-frequency mode with a very large Huang−Rhy factor, many configurations could have FCFs of similar magnitude. In this case, more configurations are needed to be sampled, so the efficiency decreases. The width of the sampled spectrum can be evaluated through the corrected sample standard deviation $s = \sqrt{\frac{1}{\Omega-1}\sum_{i=1}^{\Omega}(E_i - E_\mu)^2}$, where E_i is the emission/absorption energy on the spectrum for the configuration from ith sample. $(\Omega-1)s^2/\sigma^2$ is in a chi-squares distribution, which has only one parameter, Ω. Its confidence interval at a designated confidence level (for example, 95%) is only determined by the sampling times as $U_{min}(\Omega) < (\Omega-1)s^2/\sigma^2 < U_{max}(\Omega)$. Thus, we take the sampling times required should hold still to keep s/σ in a constant confidence interval in different systems.

Moreover, for classical sampling we found the sampling efficiency becomes lower in larger systems, probably from its two-step procedure. Meanwhile, the ECS helps to increase the efficiency for those larger systems. A numerical example for the ECS to increase the efficiency has been shown in the Supporting Information.

ASSOCIATED CONTENT

Supporting Information

The Supporting Information is available free of charge at https://pubs.acs.org/doi/10.1021/acs.jpclett.2c01475.

Benchmark of sign approximation method, physical parameters of two-mode Morse mode, physical parameters of pyridine, computational details to perform the HQCS calculation, computational details to perform the TD-DMRG reference, reference spectrum of pyridine with all 27 vibrational modes, expression of the Doktorov operator $\hat{\mathbf{U}}_{Dok}$, and a discussion on enhanced classical sampling (PDF)

AUTHOR INFORMATION

Corresponding Author

Zhigang Shuai − *MOE Key Laboratory of Organic OptoElectronics and Molecular Engineering, Department of Chemistry, Tsinghua University, Beijing 100084, People's Republic of China;* orcid.org/0000-0003-3867-2331; Email: zgshuai@tsinghua.edu.cn

Authors

Yuanheng Wang − *MOE Key Laboratory of Organic OptoElectronics and Molecular Engineering, Department of Chemistry, Tsinghua University, Beijing 100084, People's Republic of China;* orcid.org/0000-0002-4683-1614

Jiajun Ren − *MOE Key Laboratory of Organic OptoElectronics and Molecular Engineering, Department of Chemistry, Tsinghua University, Beijing 100084, People's Republic of China;* Present Address: (J.R.) Key Laboratory of Theoretical and Computational Photochemistry, Ministry of Education, College of Chemistry, Beijing Normal University, Beijing 100875, People's Republic of China; orcid.org/0000-0002-1508-4943

Weitang Li − *MOE Key Laboratory of Organic OptoElectronics and Molecular Engineering, Department of Chemistry, Tsinghua University, Beijing 100084, People's Republic of China*

Complete contact information is available at: https://pubs.acs.org/10.1021/acs.jpclett.2c01475

Notes

The authors declare no competing financial interest.

ACKNOWLEDGMENTS

This work is supported by the National Natural Science Foundation of China Grant No. 21788102 and by the Ministry of Science and Technology of China through the National Key R&D Plan Grant No. 2017YFA0204501

REFERENCES

(1) Feynman, R. P. Simulating physics with computers. *Int. J. Theor. Phys.* **1982**, *21*, 467−488.

(2) Shor, P. Algorithms for quantum computation: discrete logarithms and factoring. *Proceedings 35th Annual Symposium on Foundations of Computer Science*; IEEE: 1994; pp 124−134.

(3) Abrams, D. S.; Lloyd, S. Quantum Algorithm Providing Exponential Speed Increase for Finding Eigenvalues and Eigenvectors. *Phys. Rev. Lett.* **1999**, *83*, 5162−5165.

(4) Peruzzo, A.; McClean, J.; Shadbolt, P.; Yung, M.-H.; Zhou, X.-Q.; Love, P. J.; Aspuru-Guzik, A.; O'Brien, J. L. A variational eigenvalue solver on a photonic quantum processor. *Nat. Commun.* **2014**, *5*, 4213.

(5) Arute, F.; Arya, K.; Babbush, R.; Bacon, D.; Bardin, J. C.; Barends, R.; Biswas, R.; Boixo, S.; Brandao, F. G. S. L.; Buell, D. A.; et al. Quantum supremacy using a programmable superconducting processor. *Nature* **2019**, *574*, 505−510.

(6) Aaronson, S.; Arkhipov, A. The Computational Complexity of Linear Optics. *Proceedings of the Forty-Third Annual ACM Symposium on Theory of Computing*; ACM: New York, NY, USA, 2011; pp 333−342.

(7) Wang, H.; Qin, J.; Ding, X.; Chen, M.-C.; Chen, S.; You, X.; He, Y.-M.; Jiang, X.; You, L.; Wang, Z.; et al. Boson Sampling with 20 Input Photons and a 60-Mode Interferometer in a 10^{14}-Dimensional Hilbert Space. *Phys. Rev. Lett.* **2019**, *123*, 250503.

(8) Hamilton, C. S.; Kruse, R.; Sansoni, L.; Barkhofen, S.; Silberhorn, C.; Jex, I. Gaussian Boson Sampling. *Phys. Rev. Lett.* **2017**, *119*, 170501.

(9) Zhong, H.-S.; Wang, H.; Deng, Y.-H.; Chen, M.-C.; Peng, L.-C.; Luo, Y.-H.; Qin, J.; Wu, D.; Ding, X.; Hu, Y.; et al. Quantum computational advantage using photons. *Science* **2020**, *370*, 1460−1463.
(10) Zhong, H.-S.; Deng, Y.-H.; Qin, J.; Wang, H.; Chen, M.-C.; Peng, L.-C.; Luo, Y.-H.; Wu, D.; Gong, S.-Q.; Su, H.; et al. Phase-Programmable Gaussian Boson Sampling Using Stimulated Squeezed Light. *Phys. Rev. Lett.* **2021**, *127*, 180502.
(11) Madsen, L. S.; Laudenbach, F.; Askarani, M. F.; Rortais, F.; Vincent, T.; Bulmer, J. F. F.; Miatto, F. M.; Neuhaus, L.; Helt, L. G.; Collins, M. J.; et al. Quantum computational advantage with a programmable photonic processor. *Nature* **2022**, *606*, 75−81.
(12) Bulmer, J. F. F.; Bell, B. A.; Chadwick, R. S.; Jones, A. E.; Moise, D.; Rigazzi, A.; Thorbecke, J.; Haus, U.-U.; Van Vaerenbergh, T.; Patel, R. B.; et al. The boundary for quantum advantage in Gaussian boson sampling. *Sci. Adv.* **2022**, *8*, No. eabl9236.
(13) Deshpande, A.; Mehta, A.; Vincent, T.; Quesada, N.; Hinsche, M.; Ioannou, M.; Madsen, L.; Lavoie, J.; Qi, H.; Eisert, J.; et al. Quantum computational advantage via high-dimensional Gaussian boson sampling. *Sci. Adv.* **2022**, *8*, No. eabi7894.
(14) Reimers, J. R. A practical method for the use of curvilinear coordinates in calculations of normal-mode-projected displacements and Duschinsky rotation matrices for large molecules. *J. Chem. Phys.* **2001**, *115*, 9103−9109.
(15) Peng, Q.; Yi, Y.; Shuai, Z.; Shao, J. Excited state radiationless decay process with Duschinsky rotation effect: formalism and implementation. *J. Chem. Phys.* **2007**, *126*, 114302.
(16) Santoro, F.; Lami, A.; Improta, R.; Bloino, J.; Barone, V. Effective method for the computation of optical spectra of large molecules at finite temperature including the Duschinsky and Herzberg−Teller effect: The Qx band of porphyrin as a case study. *J. Chem. Phys.* **2008**, *128*, 224311.
(17) Shen, Y.; Lu, Y.; Zhang, K.; Zhang, J.; Zhang, S.; Huh, J.; Kim, K. Quantum optical emulation of molecular vibronic spectroscopy using a trapped-ion device. *Chem. Sci.* **2018**, *9*, 836−840.
(18) Clements, W. R.; Renema, J. J.; Eckstein, A.; Valido, A. A.; Lita, A.; Gerrits, T.; Nam, S. W.; Kolthammer, W. S.; Huh, J.; Walmsley, I. A. Approximating vibronic spectroscopy with imperfect quantum optics. *J. Phys. B: At. Mol. Opt. Phys.* **2018**, *51*, 245503.
(19) Wang, C. S.; Curtis, J. C.; Lester, B. J.; Zhang, Y.; Gao, Y. Y.; Freeze, J.; Batista, V. S.; Vaccaro, P. H.; Chuang, I. L.; Frunzio, L.; et al. Efficient Multiphoton Sampling of Molecular Vibronic Spectra on a Superconducting Bosonic Processor. *Phys. Rev. X* **2020**, *10*, 021060.
(20) Hu, L.; Ma, Y.-C.; Xu, Y.; Wang, W.-T.; Ma, Y.-W.; Liu, K.; Wang, H.-Y.; Song, Y.-P.; Yung, M.-H.; Sun, L.-Y. Simulation of molecular spectroscopy with circuit quantum electrodynamics. *Sci. Bull.* **2018**, *63*, 293−299.
(21) Arrazola, J. M.; Bergholm, V.; Brádler, K.; Bromley, T. R.; Collins, M. J.; Dhand, I.; Fumagalli, A.; Gerrits, T.; Goussev, A.; Helt, L. G.; et al. Quantum circuits with many photons on a programmable nanophotonic chip. *Nature* **2021**, *591*, 54−60.
(22) Huh, J.; Guerreschi, G. G.; Peropadre, B.; McClean, J. R.; Aspuru-Guzik, A. Boson sampling for molecular vibronic spectra. *Nat. Photonics.* **2015**, *9*, 615−620.
(23) Jnane, H.; Sawaya, N. P. D.; Peropadre, B.; Aspuru-Guzik, A.; Garcia-Patron, R.; Huh, J. Analog Quantum Simulation of Non-Condon Effects in Molecular Spectroscopy. *ACS Photonics* **2021**, *8*, 2007−2016.
(24) Dierksen, M.; Grimme, S. An efficient approach for the calculation of Franck-Condon integrals of large molecules. *J. Chem. Phys.* **2005**, *122*, 244101.
(25) Santoro, F.; Improta, R.; Lami, A.; Bloino, J.; Barone, V. Effective method to compute Franck-Condon integrals for optical spectra of large molecules in solution. *J. Chem. Phys.* **2007**, *126*, 084509.
(26) Niu, Y.; Peng, Q.; Shuai, Z. Promoting-mode free formalism for excited state radiationless decay process with Duschinsky rotation effect. *Sci. China, Ser. B: Chem.* **2008**, *51*, 1153−1158.
(27) Lin, S.; Peng, Q.; Ou, Q.; Shuai, Z. Strong Solid-State Fluorescence Induced by Restriction of the Coordinate Bond Bending in Two-Coordinate Copper(I)−Carbene Complexes. *Inorg. Chem.* **2019**, *58*, 14403−14409.
(28) Lin, S.; Ou, Q.; Wang, Y.; Peng, Q.; Shuai, Z. Aggregation-Enhanced Thermally Activated Delayed Fluorescence Efficiency for Two-Coordinate Carbene−Metal−Amide Complexes: A QM/MM Study. *J. Phys. Chem. Lett.* **2021**, *12*, 2944−2953.
(29) Niu, Y.; Li, W.; Peng, Q.; Geng, H.; Yi, Y.; Wang, L.; Nan, G.; Wang, D.; Shuai, Z. MOlecular MAterials Property Prediction Package (MOMAP) 1.0: a software package for predicting the luminescent properties and mobility of organic functional materials. *Mol. Phys.* **2018**, *116*, 1078−1090.
(30) Petrenko, T.; Rauhut, G. A General Approach for Calculating Strongly Anharmonic Vibronic Spectra with a High Density of States: $\tilde{X}^2B_1 \leftarrow \tilde{X}^1A_1$ Photoelectron Spectrum of Difluoromethane. *J. Chem. Theory Comput.* **2017**, *13*, 5515−5527.
(31) Liang, W.; Zhao, Y.; Sun, J.; Song, J.; Hu, S.; Yang, J. Electronic Excitation of Polyfluorenes: A Theoretical Study. *J. Phys. Chem. B* **2006**, *110*, 9908−9915.
(32) Heimel, G.; Daghofer, M.; Gierschner, J.; List, E. J. W.; Grimsdale, A. C.; Müllen, K.; Beljonne, D.; Brédas, J.-L.; Zojer, E. Breakdown of the mirror image symmetry in the optical absorption/emission spectra of oligo(para-phenylene)s. *J. Chem. Phys.* **2005**, *122*, 054501.
(33) Sawaya, N. P. D.; Huh, J. Quantum Algorithm for Calculating Molecular Vibronic Spectra. *J. Phys. Chem. Lett.* **2019**, *10*, 3586−3591.
(34) Lee, C.-K.; Hsieh, C.-Y.; Zhang, S.; Shi, L. Simulation of Condensed-Phase Spectroscopy with Near-Term Digital Quantum Computers. *J. Chem. Theory Comput.* **2021**, *17*, 7178.
(35) Sparrow, C.; Martín-López, E.; Maraviglia, N.; Neville, A.; Harrold, C.; Carolan, J.; Joglekar, Y. N.; Hashimoto, T.; Matsuda, N.; O'Brien, J. L.; et al. Simulating the vibrational quantum dynamics of molecules using photonics. *Nature* **2018**, *557*, 660−667.
(36) MacDonell, R. J.; Dickerson, C. E.; Birch, C. J. T.; Kumar, A.; Edmunds, C. L.; Biercuk, M. J.; Hempel, C.; Kassal, I. Analog quantum simulation of chemical dynamics. *Chem. Sci.* **2021**, *12*, 9794−9805.
(37) Ollitrault, P. J.; Mazzola, G.; Tavernelli, I. Nonadiabatic Molecular Quantum Dynamics with Quantum Computers. *Phys. Rev. Lett.* **2020**, *125*, 260511.
(38) Lin, S.; Chang, C.; Liang, K.; Chang, R.; Zhang, J.; Yang, T.; Hayashi, M.; Shiu, Y.; Hsu, F. Ultrafast dynamics and spectroscopy of bacterial photosynthetic reaction centers. *Adv. Chem. Phys.* **2002**, *121*, 1−88.
(39) Li, G.; Rosenthal, C.; Rabitz, H. High dimensional model representations. *J. Phys. Chem. A* **2001**, *105*, 7765−7777.
(40) Bowman, J. M.; Carter, S.; Huang, X. MULTIMODE: a code to calculate rovibrational energies of polyatomic molecules. *Int. Rev. Phys. Chem.* **2003**, *22*, 533−549.
(41) Doktorov, E.; Malkin, I.; Man'Ko, V. Dynamical symmetry of vibronic transitions in polyatomic molecules and the Franck-Condon principle. *J. Mol. Spectrosc.* **1975**, *56*, 1−20.
(42) Doktorov, E.; Malkin, I.; Man'Ko, V. Dynamical symmetry of vibronic transitions in polyatomic molecules and the Franck-Condon principle. *J. Mol. Spectrosc.* **1977**, *64*, 302−326.
(43) Quesada, N. Franck-Condon factors by counting perfect matchings of graphs with loops. *J. Chem. Phys.* **2019**, *150*, 164113.
(44) Barnett, S.; Radmore, P. M. *Methods in theoretical quantum optics*; Oxford University Press: Oxford, 2002.
(45) Lin, C.-K.; Chang, H.-C.; Lin, S. H. Symmetric Double-Well Potential Model and Its Application to Vibronic Spectra: Studies of Inversion Modes of Ammonia and Nitrogen-Vacancy Defect Centers in Diamond. *J. Phys. Chem. A* **2007**, *111*, 9347−9354.
(46) Lin, C.-K.; Li, M.-C.; Yamaki, M.; Hayashi, M.; Lin, S. H. A theoretical study on the spectroscopy and the radiative and non-radiative relaxation rate constants of the $S_0{}^1A_1 - S_1{}^1A_2$ vibronic transitions of formaldehyde. *Phys. Chem. Chem. Phys.* **2010**, *12*, 11432−11444.

https://doi.org/10.1021/acs.jpclett.2c01475
J. Phys. Chem. Lett. 2022, 13, 6391−6399

(47) Deng, C.; Niu, Y.; Peng, Q.; Qin, A.; Shuai, Z.; Tang, B. Z. Theoretical study of radiative and non-radiative decay processes in pyrazine derivatives. *J. Chem. Phys.* **2011**, *135*, 014304.
(48) Light, J.; Hamilton, I.; Lill, J. Generalized discrete variable approximation in quantum mechanics. *J. Chem. Phys.* **1985**, *82*, 1400−1409.
(49) Killoran, N.; Izaac, J.; Quesada, N.; Bergholm, V.; Amy, M.; Weedbrook, C. Strawberry Fields: A Software Platform for Photonic Quantum Computing. *Quantum* **2019**, *3*, 129.
(50) Gupt, B.; Izaac, J.; Quesada, N. The Walrus: a library for the calculation of hafnians, Hermite polynomials and Gaussian boson sampling. *J. Open. Source. Softw* **2019**, *4*, 1705.
(51) Ren, J.; Li, W.; Jiang, T.; Wang, Y.; Shuai, Z. Time-dependent density matrix renormalization group method for quantum dynamics in complex systems. *WIREs Comput. Mol. Sci.* **2022**, No. e1614.
(52) Wang, Y.; Ren, J.; Shuai, Z. Evaluating the anharmonicity contributions to the molecular excited state internal conversion rates with finite temperature TD-DMRG. *J. Chem. Phys.* **2021**, *154*, 214109.
(53) Ianconescu, R.; Pollak, E. Semiclassical initial value representation study of internal conversion rates. *J. Chem. Phys.* **2011**, *134*, 234305.
(54) Wang, H.; Zhu, C.; Yu, J.-G.; Lin, S. H. Anharmonic Franck-Condon Simulation of the Absorption and Fluorescence Spectra for the Low-Lying S1 and S2 Excited States of Pyridine. *J. Phys. Chem. A* **2009**, *113*, 14407−14414.
(55) Frisch, M. J.; Trucks, G. W.; Schlegel, H. B.; Scuseria, G. E.; Robb, M. A.; Cheeseman, J. R.; Scalmani, G.; Barone, V.; Petersson, G. A.; Nakatsuji, H. et al. *Gaussian 16*, Revision C.01; Gaussian Inc.: Wallingford, CT, 2016.
(56) Sparta, M.; Toffoli, D.; Christiansen, O. An adaptive density-guided approach for the generation of potential energy surfaces of polyatomic molecules. *Theor. Chem. Acc.* **2009**, *123*, 413−429.
(57) Yamazaki, I.; Baba, H. Observation of fluorescence of pyridine in the vapor phase. *J. Chem. Phys.* **1977**, *66*, 5826−5827.
(58) Baiardi, A.; Bloino, J.; Barone, V. Simulation of Vibronic Spectra of Flexible Systems: Hybrid DVR-Harmonic Approaches. *J. Chem. Theory Comput.* **2017**, *13*, 2804−2822.
(59) Ren, J.; Shuai, Z.; Kin-Lic Chan, G. Time-Dependent Density Matrix Renormalization Group Algorithms for Nearly Exact Absorption and Fluorescence Spectra of Molecular Aggregates at Both Zero and Finite Temperature. *J. Chem. Theory Comput.* **2018**, *14*, 5027−5039.
(60) Li, W.; Ren, J.; Shuai, Z. Numerical assessment for accuracy and GPU acceleration of TD-DMRG time evolution schemes. *J. Chem. Phys.* **2020**, *152*, 024127.

https://doi.org/10.1021/acs.jpclett.2c01475
J. Phys. Chem. Lett. 2022, 13, 6391−6399